EARLY DETECTION AND LOCALIZATION OF STATOR INTER-TURN SHORT CIRCUIT FAULTS BASED ON VARIATIONAL MODE DECOMPOSITION AND DEEP LEARNING IN INDUCTION MOTOR

Asma GUEDIDI [1,*] , **Widad LAALA** [2] , **Abderrazak GUETTAF** [1] , **Ali ARIF** [1]

[1] Electrical Engineering Department, The Energy Systems Modeling Laboratory (LMSE) Laboratory, University of Biskra, B.P. 145, 07000, Biskra, Algeria.

[2] Electrical Engineering Department, The Electrical Engineering Laboratory of Biskra (LGEB), University of Biskra, B.P. 145, 07000, Biskra, Algeria.

* Corresponding author, e-mail: guedidiasma@gmail.com, s.guedidi@univ-biskra.dz

Abstract

The existing diagnostic techniques for detecting inter-turn short circuits (ITSCs) in induction motors face two primary challenges. Firstly, they suffer from reduced sensitivity, often failing to detect ITSCs when only a few turns are short-circuited. Secondly, their reliability are compromised by load fluctuations, leading to false alarms even in the absence of actual faults. To address these issues, a novel intelligent approach to diagnose ITSC fault is proposed. Indeed, this method encompasses three core components: a novel multi-sensor fusion technique, a knowledge map, and enhanced Convolutional Neural Networks (CNNs). First, the raw data collected from multiple sensors undergoes a transformation into 2D data using a novel image transformation based on Hilbert transform (HT) and variational mode decomposition (VMD), which is concatenate to a novel information map including frequency fault information and rotational speed. Then, this 3D multi information image is used as input to an improvement CNN model that apply a transfer learning for an enhanced version of SqueezNet with incorporating a novel attention mechanism module to precisely identify fault features. Experimental results and performance comparisons demonstrate that the proposed model attains high performance surpassing other Deep Learning (DL) methods in terms of accuracy. In addition, the model has consistently demonstrated its ability to make precise predictions and accurately classify fault severity, even under different working conditions.

Keywords: Convolutional Neural Networks (CNNs), deep learning, short circuit fault diagnosis, variational mode decomposition, information map.

List of Symbols/Acronyms

DL   *Deep learning.*
HT   Hilbert transform.
IM   Information map.
IMs   Induction motors.
IMF   Intrinsic mode functions.
ITSC   Interturn short-circuit.
VMD   Variational mode decomposition.

1. INTRODUCTION

In the present era, over 85% of electric motors employed in industrial settings are three-phase induction motors (IMs) [1]. Squirrel-cage induction motors are widely used in various industries and transport [2]. They are extensively utilized due to their dependability, ease of design, exceptional performance, and robust load-bearing capabilities across a wide array of applications, including manufacturing, processing, power systems, transportation, and more. Regardless of their size and capacity, these IMs are deemed indispensable components in contemporary industrial sectors where uninterrupted operation hinges upon their condition.

However, IMs often operate in demanding mechanical and electrical environments, rendering them susceptible to numerous stator and/or rotor faults. Extensive research literature underscores that stator-winding faults are the most prevalent cause of electrical machine failures. Indeed, these types of faults account for approximately 20% to 40% of failures in induction machines [3], and this number can rise up to 66% for high voltage motors.

Among the primary responsible of stator faults are interturn short-circuit (ITSC) faults, known for their critical and hazardous consequences. Typically, an ITSC fault initiates as an inconspicuous electrical contact between adjacent turns due to localized insulation deterioration induced by a combination of

thermal, electrical, mechanical, and environmental stressors. This gives rise to a high current flow in the affected turns, leading to a significant temperature increase in the afflicted region (commonly referred to as a "hot spot"). This elevated temperature can swiftly lead to additional insulation failures, ultimately culminating in a complete breakdown of the stator winding [4]. Therefore, the early detection and diagnosis of short-circuit faults occurring between turns during motor operation holds paramount significance [3]. The available ITSC diagnosis techniques can be classified into signal-processing methods, model-based methods and data-driven methods [5]. The first category uses different signal processing tools to extract the defect feature information from the raw signals, such as motor current signature analysis [6], wavelet transforms [7], empirical mode decomposition method [8], Variational mode decomposition [9], etc. Then, with a large amount of expert experience, the existed fault in such a system can be localised and diagnosed. Model based methods is the second category, which uses motor mathematical models [10], observers based model to generate features such as Kalman filter in [11], etc. The third category, which has been widely adopted in recent decades, emphasizes the utilization of data-driven intelligent approaches in machine learning. This category encompasses prominent techniques like Artificial Neural Networks (ANNs), Support Vector Machines (SVMs), and Fuzzy Logic. These approaches have gained substantial popularity due to their effectiveness in extracting valuable insights and making accurate predictions from complex datasets. However, despite their widespread use, they still face certain limitations primarily stemming from their shallow structure and the requirement of feature extraction step. These limitations have prompted researchers and engineering to explore more in the deep learning approaches to overcome these constrains and further enhance the capabilities of machine learning models. In fact, Deep learning has gained an extensive adoption and popularity in recent decades owing to its remarkable ability to extract valuable features and achieve high precision and predictions without the need of prior knowledge.

In recent years, there has been a proliferation of DL-based fault diagnosis models leveraging convolutional neural network (CNN). For instance, in research that relies on a one-dimensional convolutional neural network (1D CNN), Ibrahim et al. proposed a multichannel 1D CNN for bearing fault diagnosis [12]. Jun et al. in [13] proposed a deep transfer learning method based on 1D-CNN for rolling bearing fault diagnosis. An approach for fault classification in power assets that involves real-time processing and utilizes a 1D CNN is presented in [14]. Huang et al. proposed an enhanced ensemble empirical mode decomposition incorporating adaptive noise reduction alongside a 1D CNN Classifier, for diagnosing faults in high-speed train Bogies [15].

There are also many studies conducted using 2D convolutional neural networks, often referred to as 2D CNNs. Jinsong et al. in [16] proposed an intelligent bearing fault diagnosis method that utilizes both a conditional generative adversarial network (CGAN) and a two-dimensional convolutional neural network (2-D-CNN).

Haiyoung et al. used a CNN based transfer learning with 2D sound spectrogram analysis to detect rotor faults [17]. Pham et al. proposed time-frequency analysis and a 2D CNN with multiple outputs for diagnosing compound bearing faults [18]. In their work, Zhong et al. presented a transfer learning approach that utilizes CNN and SVM techniques for the diagnosis of gas turbine faults [19].

These techniques have been successfully applied also in the inter turn fault diagnosis. For example, Huangfu [20] converted the raw data of the three-phase stator current into input matrix and then utilized deep transfer learning to recognize inter-turn short circuit fault. Patter Huan in [21] utilize the VMD to decompose the raw signal of the permanent magnet synchronous motors. The data feature set for diagnosing the turn-to-turn short circuit fault in the CNN model in this study is derived by calculating and reorganizing the poles, peaks, and decomposition coefficients of the noisy signals. In [22], the authors use the raw signal directly into CNN to diagnose the short circuit fault in induction motor. However, although the aforementioned CNN-based methods provide great results and outperform the other convolutional methods in term of accuracy but it is shown that their performance is limited on some factors: firstly, they require a large number of the training data, which need therefore a huge memory system. Otherwise, its performance is reduced when the training data are insufficient. Secondly, most CNN approaches focus only on classifying the data but do not consider the physical phenomenon that affect the fault feature in the signal. Such as the load profile, environmental factors, and the fault mechanism. Unfortunately, the aforementioned articles and most existing DL methods such in [23] - [27] do not fully utilized the fault information mechanism or the operating conditions which is very crucial for a reliable fault diagnosis. Thirdly, in the context of ITSC monitoring data, some features are irrelevant to the fault. This is particularly evident when considering a range of electrical or mechanical signals, including stator voltages and currents, radial and axial fields, electromagnetic torques, and rotational speed. The data of these signals often show different characteristics and each signal provides its unique perspective of ITSC health condition [28]. Thus, within ITSC-centred monitoring systems, it is recommended to employ multiple sensors coupled with data fusion methodologies to attain optimal performance. Consequently, The primary scope of this work is to overcome the aforementioned obstacles that revolves around identifying electrical

faults that manifest in the stator windings of induction motors used in various industrial applications, including but not limited to blowers, centrifugal pumps, and line shafting.etc. The main novelty in this article is succinctly outlined in the ensuing key points:

1) To address data limitations and reducing the dependence of CNN on large training samples, a self-attention mechanism (SAM) combined with a novel lightweight model is proposed to diagnose and classify the ITSC faults under variable operating conditions. Compared with classical CNN model, the proposed model has significantly reduced parameters and has improved generalization ability providing high accuracy performance in the shortest possible training time, making it beneficial for online diagnosis.

2) The raw data of multiple sensors are converted to 2D data images based on novel VMD energy algorithm as optimal image coding method creating a link between computer vision and fault diagnosis. This novel method allows conserving the fault information by computing automatically its severity related to the amplitude of its energy degree embedded in the sub signals. This allows to overcome the fault feature extraction step and hence the signal will be directly subjected to 1-2D image conversion automatically.

3) To reach a promising performance in fault analysistasks. A novel information map of domain knowledge, containing rotating speed and fault characteristics mechanism for the short circuit defection, is built. Then, combined with data images to form deep learning input. This fusion method helps the proposed CNN model to extract pertinent fault features under varying operational conditions and guide it to become faster with a high accuracy.

4) The performances of the proposed network model are compared to some existing CNN models.

The remain of this article is organised as follows. Section II gives the principal theory of the proposed method and its related techniques. Section III provides a detailed illustration of the comprehensive fault diagnosis system. Section IV of this article shows the empirical verification conducted on ten datasets to establish the efficacy of the proposed model. Furthermore, comprehensive performance comparisons are included. Finally, the Conclusion is presented in Section V.

2. TEORICAL BACKGROUND

2.1 CNN

The convolutional neural network (CNN) represents a robust solution for pattern recognition and image classification tasks, eliminating the necessity for intricate feature extraction procedures. It primarily consists of fundamental and crucial layers, including convolutional, subsampling or pooling, and fully connected layers [29]. The details of each one is explained as following:

2.1.1. Convolutional layer

The convolutional layer plays a crucial role in deep learning models for pattern extraction. It applies a sum of filters to the input images in order to obtain feature maps. Each filter detects specific patterns or features present in the input. The outline of the convolution function can be given by [28]:

$$x_n^{r,k} = \psi \left(\sum_m w_n^r * x_m^{r-1} + b_n^r \right) \qquad (1)$$

where x_m^{r-1} and $x_n^{r,k}$ are respectively [32], the *mth* input of level r −1 and *nth* output feature maps of level r in the convolution process. w_n^r is the convolution kernel between the *mth* input feature map and the nth output feature map and k is the number of the kernels. b_n^r is the bias of the nth output feature maps. It can be seen that the different feature maps as input share the same kernels and bias. $*$ Denote the convolution operator, and $\psi (\cdot)$ is a nonlinear activation function, which is set to be "sigmoid" or "ReLU" [28].

2.1.2. Pooling layers

Pooling layers are spatial down-sampling layers added after the convolutional layer to gradually downscale the feature map, increase the receptive field size and reduce the number of the parameters in the model. The 2D max-pooling layer partitions a spatial image into a set of small non-overlapping 2 x 2 regions. The element at position (x_1, x_2) of the l-th 2D max-pooling layer, denoted as $v_{l,c}^{x_1,x_2}$, is given by:

$$v_{l,c}^{x_1,x_2} = \max \left(R_{l,c}^{x_1,x_2} \right) \qquad (2)$$

Where

$$R_{l,c}^{x_1,x_2} = \left\{ R_{l-1,c}^{x_1',x_2'} \mid x_1' \in \{2x_1 - 1, 2x_1\}, x_2' \in \{2x_2 - 1, 2x_2\} \right\}$$
(3)

The set $R_{l,c}^{x_1,x_2}$ contains all elements in a 2x2 sub-matrix.

2.1.3. The fully connected

The fully connected layer, also known as the dense layer or the fully connected neural network, is one of the fundamental component in deep learning models. Unlike the convolutional layer, which operates on local spatial regions, the fully connected layer connects every neuron from the previous layer to every neuron in the current layer [30]. The fully connected layer can be defined as follows:

$$v_l = f \left(g \left(v_{l-1} \right) \right) \qquad (4)$$

Where

$$g(x) = Wx + b \qquad (5)$$

The function g play the role of fully connected operator [32]. It converts a vector of m dimension to a vector of n dimension by linear transformation $W \in \Box^{n \times m}$ then, the bias $b \in \Box^n$ is added to the converted vector. $f(.)$ is the nonlinear activation

function, which is generally set to be ReLU, sigmoid, tanh or max (.,0).

2.1.4 The dropout layer

The dropout layer is commonly utilized following fully connected layers to mitigate overfitting. It can be described as an element-wise dropout layer, which is defined by the following expression [31]:

$$v_{l,c} = a_{l,c} v_{l-1,c} \qquad (6)$$

$$a_{l,c} \square B(1,0) \qquad (7)$$

where

$v_{l,c}$ is the c-th activation of the l-th dropout layer.

The $a_{l,c}$ is the coefficient which determines the value assigned to the c-th activation. If this coefficient is equal to one, $a_{l,c} = 1$, the c-th activation of the l-th layer retrains its value from the previous layer, remaining unchanged. Otherwise, the c-th activation of the l-th layer is set to zero, effectively suppressing its influence from the previous layer [32].

2.2. Variational Mode Decomposition:

The Variational Mode Decomposition (VMD) algorithm is a novel technique for signal segmentation that has gained recent attention due to its advantages in dealing with signals under non-stationary and highly noisy condition. This approach incorporates three techniques: Wiener filtering, one-dimensional Hilbert transform, and heterodyne demodulation [31]. In contrast to empirical EMD, VMD can segmented the original signal into a series of its constituent (IMFs) called modes (u_k) by resolving a constrained variational problem. It considers each intrinsic mode (IMF) as an amplitude-modulated and frequency modulated (AM-FM) signal, wich characterized by a band-limited around a center frequency (ω_k). The formulation of the constrained variational problem is presented as follows [33]:

$$\min_{\{\ddot{u}_k\}\{\ddot{}\omega_k\}} \left\{ \sum_{k=1}^{k} \left\| \partial_t \left[\left(\delta(t) + \frac{j}{\pi t} \right) * u_k(t) \right] e^{-j\bar{\omega}_{kn}t} \right\|_2^2 \right\} \quad (8)$$

$$\sum_{k=1}^{k} u_k(t) = f(t) \qquad (9)$$

In order to resolve the problem defined in (8), the augmented Lagrangian method was used. Consequently, the non-constrained variational problem can be given by the following expression [31]:

$$L(\{u_k\},\{\omega_k\},\lambda) \ddot{} = \alpha \left\{ \sum_{k=1}^{\ddot{}k} \left\| \partial_t \left[\left(\delta(t) + \frac{j}{\pi t} \right) * u_k(t) \right] e^{-j\omega_k t} \right\|_2^2 \quad (10) \right.$$

By utilizing the alternate direction method of multipliers (ADMM), the iterative equations for u_k and ω_k can be obtained. In this context, α

represents the balancing parameter that controls the data fidelity constraint, while $\lambda(t)$ corresponds to the Lagrange multipliers. The expressions for u_k, ω_k and λ in the iterative process are given as follows [32]:

$$u_k^{n+1}(\omega) = \frac{f(\omega) - \sum_{i<k} u_k^{n+1}(\omega) - \sum_{i>k} u_k^n(\omega) + \frac{\lambda^n(\omega)}{2}}{1 + 2\alpha(\omega - \omega_k^n)^2} \quad (11)$$

$$\omega_k^{n+1} = \frac{\int_0^\infty \omega \left| u_k^{n+1}(\omega) \right|^2 d\omega}{\int_0^\infty \left| u_k^{n+1}(\omega) \right|^2 d\omega} \qquad (12)$$

$$\lambda^{n+1} = \lambda^n + \tau \left(f - \sum_k u_k^{n+1} \right) \qquad (13)$$

The primary steps of the VMD algorithm can be outlined as follows [34]:

Step 1: Initialize $u_k^l, \omega_k^l, \lambda_k$.

Step 2: Update u_k, ω_k related to equations (11) and (12).

Step 3: Update λ based on the equation (13).

Step 4: if $\sum_k \frac{\left\| u_k^{n+1} - u_k^n \right\|_2^2}{\left\| u_k^n \right\|_2^2} < \varepsilon$ end the iteration.

Otherwise return to step2.

2.3. Stator phase current envelope
2.3.1 Stator current in case of ITSC fault

Theoretically, in the case of healthy three-phase squirrel cage induction motor, the general expressions of stator currents can be written as:

$$\begin{cases} i_A(t) = I_f \cos(2\pi f_s t) \\ i_B(t) = I_f \cos(2\pi f_s t - \frac{2\pi}{3}) \\ i_C(t) = I_f \cos(2\pi f_s t - \frac{4\pi}{3}) \end{cases} \quad (14)$$

The occurrence of an ITSC fault provides a slight increase in the current of the injured phase accompanied by a dangerous increase in temperature, which can eventually lead to the destruction of the insulation and the winding. In [35] and [36], the authors reported that the stator current harmonics induced by the presence of an ITSC fault could be defined by:

$$f_{ITSC} = f_s \pm k f_r \qquad (15)$$

Where f_{ITSC}, f_s and f_r are the inter-turn short-circuit harmonics, the supply frequency and the speed rotation frequency. Therefore, in the case of ITSC fault, the stator currents expression can be given by:

$$i_A(t) = I_f \cos(2\pi f_s t) +$$

$$\sum_k I_{ITSC1}^k \cos(2\pi(f_s - kf_R)t - \varphi_{ITSC1}^k) + \qquad (16)$$

$$\sum_k I_{ITSC2}^k \cos(2\pi(f_s + kf_R)t - \varphi_{ITSC2}^k)$$

$$i_B(t) = I_f \cos(2\pi f_s t - \frac{2\pi}{3})$$

$$+ \sum_k I_{ITSC1}^k \cos(2\pi(f_s - kf_R)t - \varphi_{ITSC1}^k) \qquad (17)$$

$$+ \sum_k I_{ITSC2}^k \cos(2\pi(f_s + kf_R)t - \varphi_{ITSC2}^k)$$

$$i_B(t) = I_f \cos(2\pi f_s t - \frac{2\pi}{3})$$

$$+ \sum_k I_{ITSC1}^k \cos(2\pi(f_s - kf_R)t - \varphi_{ITSC1}^k) \qquad (18)$$

$$+ \sum_k I_{ITSC2}^k \cos(2\pi(f_s + kf_R)t - \varphi_{ITSC2}^k)$$

Where, I_f, I_{ITSC1}^k, I_{ITSC2}^k denote, respectively, the fundamental amplitudes and the sideband harmonic related to the ITSC fault.

2.3.2 Stator current envelope (SCE)

The envelope signal is obtained using a process called envelope detection or amplitude demodulation. This process involves extracting the magnitude variations of a signal (such as an amplitude-modulated signal) to obtain the envelope signal, that contain the main fault valuable information, through the application of Hilbert transform on the raw signal. In case of ITSC fault, the signal envelope is mathematically defined in (21). In fact, the equation (16) of the first stator phase current can be rewritten as:

$$i_A(t) = A(t) \cos(2\pi f_s t) + B(t) \sin(2\pi f_s t) \quad (19)$$

(19) Can take the following form:

$$i_A(t) = A_m(t) \sin(2\pi f_s t + \theta(t)) \qquad (20)$$

With

$$A_m(t) = \sqrt{A(t)^2 + B(t)^2} , \qquad (21)$$

$$\theta(t) = \arctan\left(\frac{A(t)}{B(t)}\right)$$

$$A(t) = I_f + \sum_k (I_{ITSC1}^k \cos(\varphi_{ITSC1}^k) + I_{ITSC2}^k \cos(\varphi_{ITSC2}^k)) \cos(2\pi kf_r)t$$

$$+ (I_{ITSC1}^k \sin(\varphi_{ITSC1}^k) - I_{ITSC2}^k \sin(\varphi_{ITSC2}^k)) \sin(2\pi kf_r)t \quad (22)$$

$$B(t) = I_f + \sum_k (I_{ITSC1}^k \sin(\varphi_{ITSC1}^k) + I_{ITSC2}^k \sin(\varphi_{ITSC2}^k)) \cos(2\pi kf_r)t$$

$$+ (I_{ITSC1}^k \cos(\varphi_{ITSC1}^k) - I_{ITSC2}^k \cos(\varphi_{ITSC2}^k)) \sin(2\pi kf_r)t \quad (23)$$

As shown in previous relations (22) and (23), the imbalanced stator phases induced by the ITSC fault leads to the amplitude modulation of the stator current at frequency kf_r. This effect allows the stator current envelope (SCE) to be served as a merit diagnostic signal [36].

2.3.3 Extraction of SCE

Usually, the SCE can be obtained by Hilbert transform (HT), which is a well-established method extensively employed in the field of signal analysis. Mathematically, the HT of stator current $i_A(t)$ can be given by [40] :

$$HT(i_A(t)) = y(t) = \frac{1}{\pi t} * i_A(t)$$
$$= \frac{1}{\pi} \int_{-\infty}^{+\infty} \frac{i_A(\xi)}{(t - \xi)} d\xi \qquad (24)$$

The SCE can be extracted by the resulting expression:

$$SCE(t) = \sqrt{i_A(t)^2 + y(t)^2} \qquad (25)$$

3. PROPOSED METHOD

3.1 Problematic issue

Short circuit faults in stator windings are widely acknowledged as the primary cause of failure in electrical machines. The detection of this fault is very challenging. In fact, even a small number of shorted turns can lead to significant issues. It can produce a tragic breakdown not only within the motor itself but also in its associated equipment. However, when a short circuit fault occur even for a low fault severity, it will affect the magnitude of the f_{ITSCH} harmonic as reported in [32], |36]. The advantage of this frequency is it characterize the fault of the short circuit frequency signature in the low frequency band that helps to discern between the faulty and healthy state. However, the challenging aspect of diagnosing this fault is that a very small number of turns in short circuit cannot be directly detected from the raw signal. To overcome this problem, Deep learning and advanced pre-processing data method can provide a solution to resolve this issue. The primary advantage of applying deep learning in fault diagnosis is that it can solve the aforementioned problem by treating signals or specific faults as unique image representations. However, regarding the study of this fault. Most DL approaches does not integrate its localisation or severity estimation. To overcome this problem, this paper propose a novel information map to integrate the domain knowledge, fault frequency signature localization and fault severity estimation, which constitute the first great novelty of this article. To accomplish these tasks. The overview of this method is presented in Figure 1. The raw signal was selected

for three different sensor localisation and then are processed through a novel signal to image conversion algorithm. The advantage of this signal-image algorithm is to highlights the energy fluctuation in different degree to get a different fault severity estimation. However, in this work, the 2D data are concatenated with the novel IM to create the input images to the improvement CNN. Details are provided in following sections.

3.2 Encoding time-series signal into image

In the domain of machine fault diagnosis, stator current signals are commonly known for their complex nature, often containing a significant volume of extraneous information that is unrelated to the diagnosis of faults. [36]. Fortunately, Convolutional Neural Networks (CNNs) are specifically tailored to handle highly nonlinear and complex signals, which proves advantageous in the field of machine fault diagnosis when dealing with intricate stator current signals.; this is due to its convolution
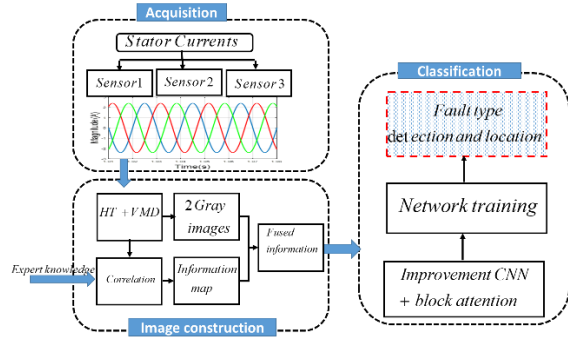
Fig. 1. Flow chart of the proposed method

operation, which works similar to a filter (e.g., lowpass, bandpass, or high pass).Thus, this means that the CNN is able to extract strong and distinguishable features from complex higher-dimensional structure, such as 2D/3D images. For this purpose, a new image is constructed by fusion of the data 2 Gray images with the IM as shown in figure 2. In fact, a set of overlapping windows of length M is utilized to segment each stator phase current data into M segments. Then, each segment was processed using the HT and VMD methods. In fact, the VMD is carried out on each segment, in order to segment the signals into IMF sub-signals. Then, the stored IMF energy can be computed as:

$$E_i = \sum_{n=1}^{M} \left[U_i(n) \right]^2 \quad i = 1, 2, \ldots, N \qquad (26)$$

Where U_i represents the IMF signal, N and M are respectively the length signal and the mode number.

By using both the energy of the IMFs and its signals, the 2D data matrix of size (MxN) is built. In this paper, this matrix is called Energy IMF signals (EIS), and it can be constructed as follows:

$$EIS\big|_{i,j}^{\tau} = E_{i..} + U_{i,j}^2 \; ; \; i = 1, 2, \ldots, M \quad j = 1, 2, \ldots, N \quad (27)$$

The ith vector into WSE matrix is set as:

$$EIS_i = \left[y_i(1), y_i(1), \ldots, y_i(N) \right] \qquad (28)$$

Where:

$$y_i(j) = E_i + U_i^2(j) \qquad (29)$$

According to (27), at each time delay τ an EIS matrix is constructed which represents the energy fluctuation of the various obtained sub-signals. In this case, the dynamic nature of the frequency distribution can be mapped into EIS matrix that can hold a fixed number of feature descriptors, thus reducing the computational complexity of the texture-based fault. Finally, a 2D data image is constructed, characterized by its size of M×N. The EIS matrix values are scaled and normalized between 0 and 255, reflecting the grayscale pixel intensity values of the Gray image. By considering EIS (i, j) as the energy value, the image (D) pixel intensity at the coordinates (i, j) $i, j \in \left[1, \ldots, M \right]$ can be expressed as follows:

$$D(i, j) = round \left\{ \frac{255}{I_{max} - I_{min}} \left[EIS(i, j) - I_m \right] \right\} (30)$$

Where I_{max} and I_{min} denote the maximum and minimum of the energy values of the IMFs.
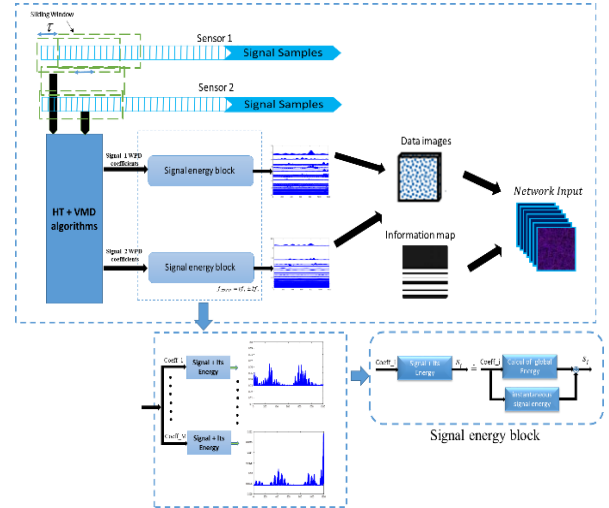

Fig. 2. Time-series signal into image conversion process

3.3. Information map construction

An information map (IM) is a visual representation of data or knowledge that provides a structured and organized view of the information. It typically includes various expert domain knowledge about a particular discipline or field like fault characteristics, operating condition and some diagnosis rules that can be deduced from historical observing data, etc [37]. For ITSC fault diagnosis, one of the prominent significant type of domain-

specific knowledge is the frequency fault characteristics (FCF).

As mentioned above, eq (15) can be rewrite as:

$$f_{ITSC} = \frac{1}{1-g} f_r \pm k f_r = k_{FCF} f_r \quad (31)$$

With

$$k_{FCF} = \frac{1}{1-g} \pm k = f_r, \quad k = 1, 2, \dots \quad , \text{ and g is the}$$

slip.

It is obvious that the FCF can be determined if both shaft speed and slip are available. However, it is well known that the impact of these frequencies is existed on the low area. To reinforce the DL bearing diagnosis in this range, an information map (IM) is constructed to merge, among other things, the domain knowledge in the networks input. To preserve the IM data coherent with the resulting data images, several operating conditions are displayed in different gray scales. Initially, the IM is constructed as an empty matrix of size M ×M. then, the IM background refers to the representation of operating condition information through gray levels [32], denoted as y_{ij} :

$$y_{ij} = \Delta f_r \quad (32)$$

Where y_{ij} is the gray value at the specified coordinate (i, j), Δf_r is the discretized rotating speeds. The main steps to construct the information map are recapitulated as follows.

1. Acquisition of stator currents from multiple sensors for different operating conditions including the record of speed and the load.
2. Extract the stator current envelope of each signal phase.
3. Segment the envelope signal into an aggregation sub-signals using VMD
4. Calculate the correlation quantities, according to (34), between the resulted sub-signals and the synthetic signals defined as:

$$S_i(t) = A_i \sin(2\pi k_{FCFi} f_r t) \quad (33)$$

$$r_{S,U_i} = \left| \frac{\sum_{i=1}^{M} (S - \overline{S})(U_i - \overline{U}_i)}{\sigma_S \sigma_{U_i}} \right| \quad (34)$$

5. The most correlated signals, according to a predefined threshold, are chosen to construct the information map at coordinate:

$$i_{FCF_d} = round\left(i_{fr} \frac{k_{FCF_d} \Delta f_r}{\Delta f_{FCF}} \right) \quad (35)$$

Where $d = 1, 2, 3 \dots$, k_{FCF_d} and Δf_{FCF} represents the index, the coefficient and the discretization step of the FCFs, which are f_{ITSC}, Δf_r . i_{FCF_d} and i_{fr} corresponding to the horizontal coordinates of the FCF and the rotating speed on the information map respectively

Finally, the built information map is combined with the data images to construct the input network. Then, the obtained image is resized to (227x227x3). Fig.3 illustrates the images related to three type of states (healthy and with ITSC fault).

3.4. Overview of SqueezNet

Over the past few years, the integration of lightweight models has greatly enhanced the efficiency of neural networks, allowing them to be applied to a diverse set of tasks.
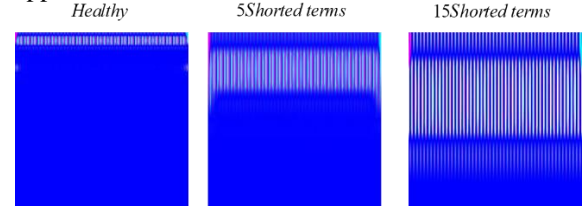

Fig. 3. The resulted input images for healthy and fault states

This advancement has been facilitated by the emergence of innovative lightweight architecture designs like SqueezeNet, MobileNet, and ShuffleNet. Among these, SqueezeNet particularly stands out as a model with lower complexity that achieves comparable accuracy to AlexNet but with a significantly reduced parameter count of just 1/50th. SqueezeNet consists of a fundamental building block known as the Fire module, which incorporates both a squeeze layer and an expand layer. The squeeze layer employs 1 × 1 convolution filters, resulting in a significant reduction of parameters by a factor of nine compared to using 3 × 3 convolution filters. The expand layer utilizes a combination of 1 × 1 and 3 × 3 filters. The overall structure of SqueezeNet is composed of nine Fire modules, forming its global architecture, as shown in Fig. 4.

3.5. Proposed modified SqueezNet

Ensuring the uninterrupted operation of machines requires the presence of a crucial ITSC fault detection model. The fundamental concept of the proposed method revolves around the utilization of transfer learning to precisely locate fault features while reducing the computational load of the deep fault detection model [38]. By combining transfer learning with deep learning (DL), the proposed approach offers an efficient solution for detecting ITSC faults.

The details of the improved SqueezNet model, as shown in figure.6, is described down below:

- The SqueezNet original architecture is modified where the last four fire modules were deleted which remain only five fire modules.
- The first ReLU were deleted and replaced with leaking RELU to further speeds up the training process.
- In our classification problem, the final convolution layer of SqueezeNet is substituted with a newly tailored layer.

- A block of coordinate attention mechanism is added where the dropout layer was deleted and replaced by batchNormalisation, and the global average pooling was placed after the sum (concatenation layer) from the block of attention mechanism

The block of attention is shown in figure 7, which contains three lateral connections (f1, f2, f3). Where the f3 contained a paypass layer that is firstly extracted from the concatenation layer of the fifth fire modules to the last concatenation layer. While the f1 lateral connection contained an average pooling layer, convolution layer and clipped ReLU layer and the second f2 lateral connection contained batchNormalisation layer, convolution layer and ReLU. The aim of this block is to localize the diagnosis of the ITSC fault by focus on low frequencies area as shown in figure 5.
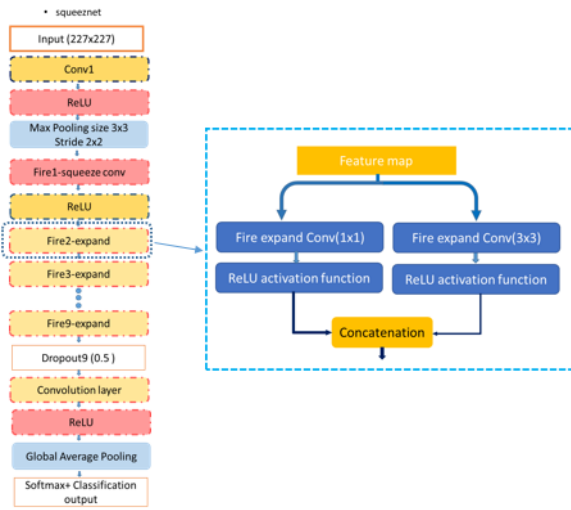
Fig. 4. SqueezNet model architecture
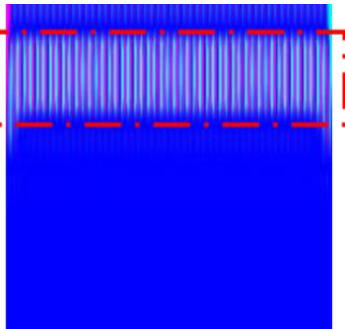
Fig. 5. The ITSC fault attention area

In this case, the horizontal direction is enough to aggregate ITSC fault features. In this direction, for a given input $X \in \mathbb{R}^{CxHxW}$, we use a spatial extent by the application of a pooling kernel (1, W) to encode each channel along the vertical coordinate leads to the formulation of the output for the c-th channel at width w as follows:

$$P(X) = \frac{1}{W} \sum_{0 \le i \le W} x_c(h,i) \qquad (36)$$

(36) facilitates the establishment of a global receptive field and effectively encodes accurate

positional information. Thus, eq (1) can be rewrite in a compact form as:

$$Conv(X) = CX + B \qquad (37)$$

Where $X \in \mathbb{R}^{CXHXW}$ and C, B represent the convolution matrix and bias respectively.
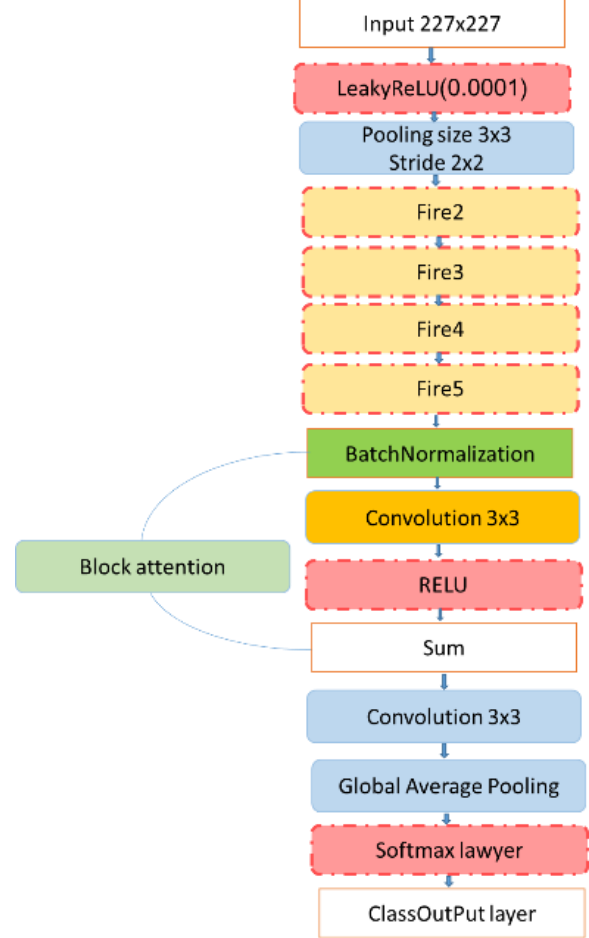

Fig. 6. The proposed modified squeeznet

The formulation for the specific value of this mechanism can be expressed as follows:

$$f_1 = \delta_1\big(conv(P(X))\big) \qquad (38)$$

$$f_2 = \delta_2\big(conv(\beta(X))\big) \qquad (39)$$

$$f = [f_1, f_2] \qquad (40)$$

The expression for the coordinate attention output can be formulated as:

$$output = [conv(f), X] \qquad (41)$$
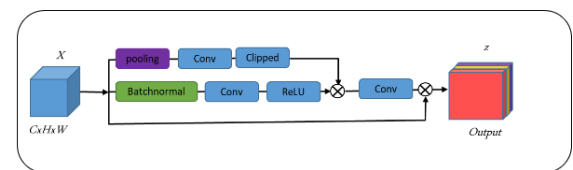

Fig. 7. Proposed coordinate block of attention mechanism

Where [·, ·] denotes the concatenation operation, δ_1, δ_2 and β are Clipped RELU, RELU activation function and batch normalisation.

4. EXPERIMENTAL RESULTS

4.1. Data Description and image construction

To evaluate the effectiveness of our diagnostic method, the proposed improvement SqueezNet is conducted on the experimental data with multiple ITSC faults and under different motor operating conditions. Fig 8 illustrates the experimental test bench utilized in this work, which is composed of a 1.1 kW squirrel-cage induction motor, an external box is incorporated to introduce ITSC faults into the stator phase, enabling the variation of the number of turns. (as shown in Fig. 9). The mechanical load consists of powder brake driven by a control unit. The currents in the three-phase stator of the induction motor were obtained through current sensors and sampled at a rate of 10 kHz using an NI 6036-E series data acquisition card.
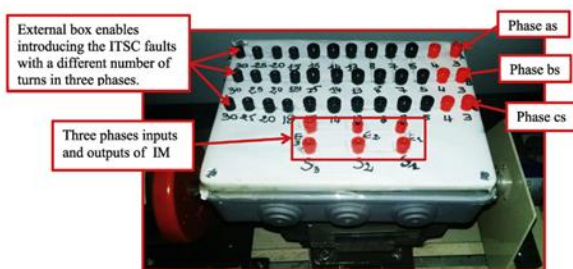

Fig. 8. The experimental setup

Fig. 9. External box with several ITSC fault

The stator current and its envelope associated to their decomposition by VMD are illustrated in Figures 10 and 11 respectively, representing both the healthy state and the condition with five shorted turns.

4.2. Performance verification

The proposed method is tested and evaluated over the 3D dataset generated using the VMD signal-to-image conversion. The modified CNN model was constructed in a MATLAB environment on a computer with two E5-2667 v3 CPUs, a GTX1080Ti GPU, 32GB of memory, and a 1TB hard drive.
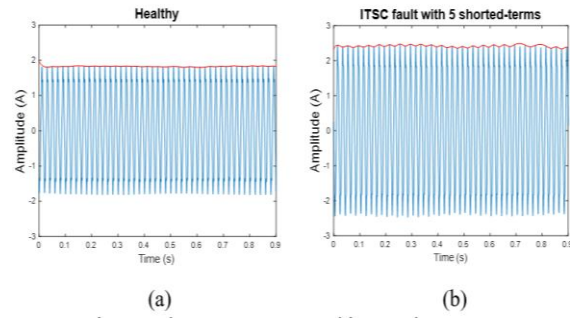

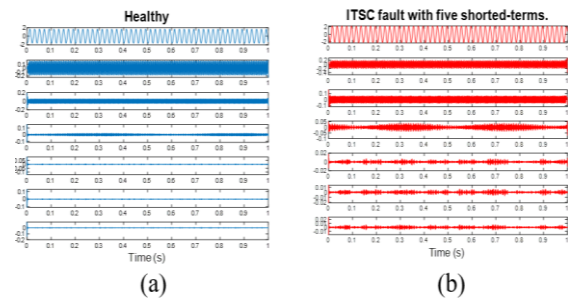Fig. 10. The stator current and its envelope a) Healthy b) ITSC fault with five shorted terms.

Fig. 11. The VMD decomposition: (a) Healthy state (b) ITSC fault with five shorted-terms (red).

However, we used ten classes (healthy and AF_a–BF_d, as registered in Table 1 to validate the CNN model. There are 300 images per class where in each case; the dataset was divided into two subsets: training and testing. The training subset comprised 70% of the data, while the remaining 30% was allocated for testing. During the training stage, the system acquired knowledge of the features, and subsequently, in the testing stage, the system performance was evaluated based on this acquired knowledge. The results of the improved CNN model with attention mechanism, in term of training and testing accuracy, is presented in Fig.12. It is evident that the proposed method demonstrates rapid convergence, ultimately creating a highly accurate model.

Additionally, to emphasize the effectiveness of the proposed technique, we utilize both the confusion matrix and T-SNE visualization, as shown in Figures 13 and 14, respectively. As illustrated in Figure 13, the diagonal entries in the matrix indicate correct classifications, whereas the off-diagonal elements represent instances of misclassification. In summary, the depiction of the confusion matrix is as follows.

The classes (AF_a, AF_b, BF_d) : ITSC with 7, 13, 20 shorted terms respectively without load. Here, the motor fault data are correctly classified. The accuracy of each class is 100%.

The classes (AF_d, AF_e, BF_a) : ITSC with 5, 7, 13, shorted terms respectively under 30% of rated load. In this case, the motor fault data are correctly

classified and an accuracy of 100% is achieved, for each class.

Table 1. Index class related to different type of fault

Index class.	Type of fault	Number of shorted terms
AF_a	ITSC_phaseA_no load	7
AF_b	ITSC_phaseA_no load	13
AF_c	ITSC_phaseA_no load	15
AF_d	ITSC_phaseA_30% of rated load	5
AF_e	ITSC_phaseA_30% of rated load	7
BF_a	ITSC_phaseA_30% of rated load	13
BF_b	ITSC_phaseA_no load	20
BF_c	ITSC_phaseA_50% of rated load	13
BF_d	ITSC_phaseA_50% of rated load	15

The classes (BF_c, BF_d): ITSC with 13 and 15 shorted terms respectively under 50% of rated load. For these two classes, the motor fault data are correctly classified and an accuracy of 100% is attained.

The class AF_c: ITSC with 15 shorted terms, without load. The number of misclassified data is 2. An accuracy of 97.8% (90/92) is achieved.

In the case of a healthy motor condition (Healthy), all the data is accurately classified, achieving 100% accuracy.

In total, there are 896 data points correctly classified out of a total of 898. Therefore, the overall accuracy of the proposed method stands at 99.8% (896/898).
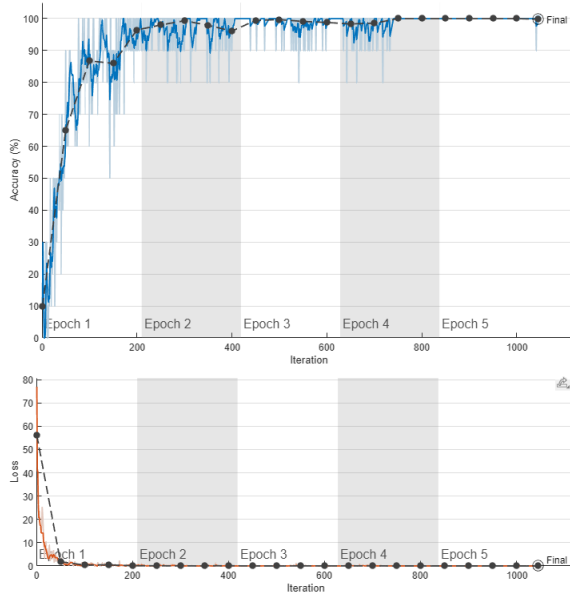

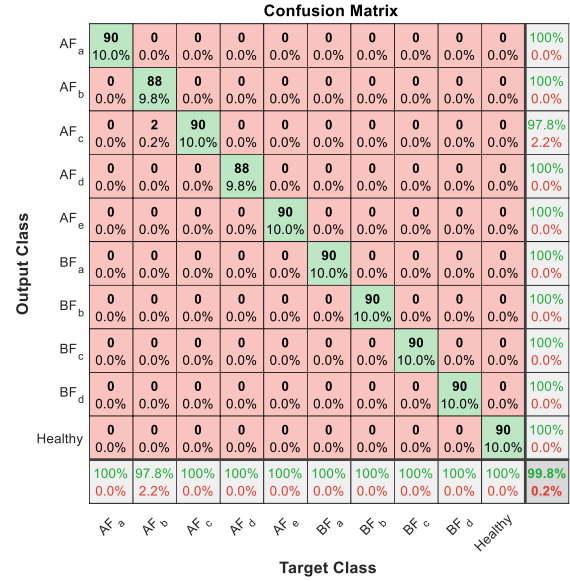Fig. 12. Accuracy training and testing of the proposed CNN
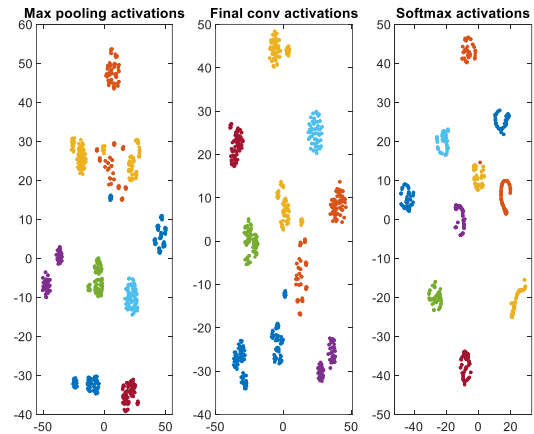

Fig. 13. Confusion matrix

Fig.14. T-SNE visualization

Overall, we can confirmed that the model has correctly predicted and classified the fault severity even under different conditions, which is also consistent with the T-SNE visualization as well. In fact, the final feature results obtained for the testing data from datasets AF_a to BF_d are displayed in figure 14. Observing the graphs, it is evident that the feature distributions corresponding to the same health conditions are notably compact or tightly clustered. While features related to different health conditions are distinctly separated in these ten different datasets. To conclude, the proposed model demonstrate robust identifiability and reliability in diagnosing ITSC fault under various working conditions.

4.3. Performance comparison

Table 2 presents a thorough comparison highlighting the fault diagnosis accuracy of four established deep learning (DL) algorithms that utilize Convolutional Neural Networks (CNN), which is AlexNet, MobileNet, RasNet-50 and the standard SqueezNet.

Table 2. Comparison with DL algorithms

Index class.	Type of fault	consuming time [s]
Proposed method	99.8%	56
Squeeznet	99.3%	50
Mobilenet	99.7%	72
Alexnet	99.5%	72
RESNET50	99.7%	60

Indeed, the results distinctly indicate that the proposed model achieves similar accuracy performance and speed when compared to renowned models

CONCLUSION

This article introduced an innovative deep learning approach tailored for the diagnosis and localization of inter-short circuit faults. Our method involved the development of a data fusion approach, leveraging the HT and VMD, to combine current signals from multiple sensors with domain knowledge and operating conditions. This fused multi-dimensional information was subsequently used to train the improvement CNN model in a unified training process.

The refined CNN model combined with multi-dimensional data including domain knowledge related to fault characteristic frequency and rotational speed, proves highly effective in accomplishing ITSC fault diagnosis for different operating condition and fault severity.

The suggested model combines the self-attention mechanism with the CNN network, resulting in a promising performance in fault analysis tasks. Given the limited availability of data in the practical domain, the self-attention mechanism proves highly advantageous as it can effectively utilize the limited data resources by highlighting the most relevant regions within the CNN input image.

The method was tested experimentally using a setup involving ten different conditions. The results strongly demonstrate the significant potential of our proposed method in improving the accuracy of fault diagnosis. Through the fine-tuning of hyper parameters, we achieve a CNN model with an accuracy of 99.8%.

Furthermore, the utilization of both the confusion matrix and the t-SNE method serves to visualize the CNN learning process. These results collectively underscore the efficacy of the proposed method in accurately diagnosing ITSC faults under different loads.

Author contributions: *research concept and design, As.G., W.L.; Collection and/or assembly of data, As.G., W.L.; Data analysis and interpretation, As.G., W.L.; Writing the article, As.G.; Critical revision of the article, As.G., W.L., Ab.G.; Final approval of the article, As.G., Ab. G., A.A.*

REFERENCES

1. Lee H, Jeong H, Koo G, Ban J, Kim SW. Attention recurrent neural network-based severity estimation method for interturn short-circuit fault in permanent magnet synchronous machines. IEEE Transactions on Industrial Electronics 2020; 68(4): 3445-3453. https://doi.org/10.1109/TIE.2020.2978690.

2. Gerlici J, Goolak S, Gubarevych O, Kravchenko K, Kamchatna-Stepanova K, Toropov A. Method for determining the degree of damage to the stator windings of an induction electric motor with an asymmetric power system. Symmetry 2022; 14(7): 1305. https://doi.org/10.3390/sym14071305.

3. Alloui A, Laadjal K, Sahraoui M, Cardoso AJM. Online interturn short-circuit fault diagnosis in induction motors operating under unbalanced supply voltage and load variations, using the STLSP Technique. IEEE Transactions on Industrial Electronics 2022; 70(3): 3080-3089. https://doi.org/10.1109/TIE.2022.3172751.

4. Gubarevych O, Goolak S, Melkonova I, Yurchenko M. Structural diagram of the built-in diagnostic system for electric drives of vehicles. Diagnostyka 2022; 23(4): 2022406. https://doi.org/10.29354/diag/156382.

5. Guangxing N, Enhui L, Xuan W, Paul Z, Bin Z. Enhanced discriminate feature learning deep residual CNN for multitask bearing fault diagnosis with information fusion. IEEE Transactions on Industrial Informatics 2023; 19(1): 762-770. https://doi.org/10.1109/TII.2022.3179011.

6. Mejia-Barron A, Tapia-Tinoco G, Razo-Hernandez JR, Valtierra-Rodriguez M, Granados-Lieberman D. A neural network-based model for MCSA of inter-turn short-circuit faults in induction motors and its power hardware in the loop simulation. Computers & Electrical Engineering., 2021; 93: 107234. https://doi.org/10.1016/j.compeleceng.2021.107234.

7. Zhang Z, Ma J, Xiangli K, Ma Y, Gong X, Xu J. Diagnosis of Inter-Turn Short Circuit Fault Based on Wavelet Transform and PSO-SVM. 2021 6th International Conference on Transportation Information and Safety (ICTIS) 2021; 1025-1028. https://doi.org/10.1109/ICTIS54573.2021.9798685.

8. Çetin M, Sarica Y. Artificial Intelligence Based Game Levelling. Balkan Journal of Electrical and Computer Engineering 2020; 8(2): 147-153 https://doi.org/10.17694/bajece.650484

9. Huang J, Lin R, He Z, Song H, Huang X, Chen B. Application of WOA-VMD-SVM in fault diagnosis of generator inter-turn short circuit. 2022 China Automation Congress (CAC). IEEE, 2022. https://doi.org/10.1109/CAC57257.2022.10055106.

10. Bachir S, Tnani S, Trigeassou JC, Champenois G. Diagnosis by parameter estimation of stator and rotor faults occurring in induction machines. IEEE Transactions on Industrial Electronics 2006; 53(3): 963-973. https://doi.org/10.1109/TIE.2006.874258.

11. Aubert B, Régnier J, Caux S, Alejo D. Kalman-Fiter-based indicator for online interturn short circuits detection in permanent-magnet synchronous generators. IEEE Transactions on Industrial

Electronics 2015;62(3):1921-1930. https://doi.org/10.1109/TIE.2014.2348934.

12. Ozgan IH, Devecioglu OC, Ince T, Askar M. Enhanced bearing fault detection using multichannel, multilevel 1D CNN classifier. Electrical Engineering 2022; 104: 435-447. https://doi.org/10.1007/s00202-021-01309-2.

13. He J, Li X, Chen Y, Chen D, Guo J, Zhou Y. Deep transfer learning method based on 1D-CNN for bearing fault diagnosis. Shock and Vibration 2021; 1-16. doi.org/10.1155/2021/6687331.

14. Imene M, Nesbitt A, Conner S, Boreham P, Morison G. 1D-CNN based real-time fault detection system for power asset diagnostics. IET Generation, Transmission & Distribution 2020; 14(24): 5766-5773. https://doi.org/10.1049/iet-gtd.2020.0773.

15. Huang D, Li S, Qin N, Zhang Y. Fault diagnosis of high-speed train bogie based on the improved-CEEMDAN and 1-D CNN algorithms. IEEE Transactions on Instrumentation and Measurement 2021; 70: 1-11. https://doi.org/10.1109/TIM.2020.3047922.

16. Jinsong Y, Liu J, Xie J, Wang C, Ding T. Conditional GAN and 2-D CNN for bearing fault diagnosis with small samples. IEEE Transactions on Instrumentation and Measuremen*t* 2021; 70: 1-12. https://doi.org/10.1109/TIM.2021.3119135.

17. Haiyoung J, Choi S, Lee B. Rotor fault diagnosis method using CNN-Based transfer learning with 2D sound spectrogram analysis. Electronics 2023; 12(3): 480. https://doi.org/10.3390/electronics12030480.

18. Pham MT, Kim JM, Kim CH. 2D CNN-based multi-output diagnosis for compound bearing faults under variable rotational speeds. Machines 2021; 9(9): 199. https://doi.org/10.3390/machines9090199.

19. Zhong, SS, Fu S, Lin L. A novel gas turbine fault diagnosis method based on transfer learning with CNN. Measurement 2019; 137: 435-453. https://doi.org/10.1016/j.measurement.2019.01.022.

20. Huangfu, H., Zhou, Y., Zhang, J., Ma, S., Fang, Q., & Wang, Y. Research on inter-turn short circuit fault diagnosis of electromechanical actuator based on transfer learning and VGG16. Electronics;2022, 11(8), 1232.https://doi.org/10.3390/electronics11081232.

21. Huan S, Li J, Zhang Y, Wang Q. VMD-CNN: Dual feature extraction for detection of turn-to-turn short circuit faults in permanent magnet synchronous motors. Proceedings of the 2022 6th International Conference on Computer Science and Artificial Intelligence 2022; 224-230. https://doi.org/10.1145/3577530.3577566.

22. Skowron M, Orłowska-Kowalska T, Wolkiewicz M, Kowalski CT. Convolutional neural network-based stator current data-driven incipient stator fault diagnosis of inverter-fed induction motor. Energies 2020; 13(6), 1475. https://doi.org/10.3390/en13061475.

23. Laohu Y Lian D, Kang X, Chen Y, Zhai K. Rolling bearing fault diagnosis based on convolutional neural network and support vector machine. IEEE Access 2020; 8: 137395-137406. https://doi.org/10.1109/ACCESS.2020.3012053.

24. Guo S, Yang T, Gao W, Zhang C. A novel fault diagnosis method for rotating machinery based on a convolutional neural network. Sensors 2018; 18(5):1429. https://doi.org/10.3390/s18051429.

25. Moradzadeh A, Moayyed H, Mohammadi-Ivatloo B, Gharehpetian GB, Aguiar AP. Turn-to-turn short

circuit fault localization in transformer winding via image processing and deep learning method. IEEE Transactions on Industrial Informatics 2021; 18(7): 4417-4426. https://doi.org/10.1109/TII.2021.3105932.

26. Liu R, Meng G, Yang B, Sun C, Chen X. Dislocated time series convolutional neural architecture: An intelligent fault diagnosis approach for electric machine. IEEE Transactions on Industrial Informatics 2016; 13(3): 1310-1320. https://doi.org/10.1109/TII.2016.2645238.

27. Wang X, Mao D, Li X. Bearing fault diagnosis based on vibro-acoustic data fusion and 1D-CNN network. Measurement 2021; 173: 108518. https://doi.org/10.1016/j.measurement.2020.108518.

28. Ding X, He Q. Energy-fluctated mulstiscale feature learning with deep convent for intelligent spindle bearing fault diagnosis. IEEE Transactions on Instrumentation and Measurement 2017, 66(8), 1926-1935. https://doi.org/10.1109/TIM.2017.2674738.

29. Jiang X, Yang S, Wang F, Shengli X, Wang X, Cheng X. OrbitNet: A new CNN model for automatic fault diagnostics of turbomachines. Applied Soft Computing 2021; 110: 107702 https://doi.org/10.1016/j.asoc.2021.107702

30. [Online]: https://medium.com/codex/understanding-convolutional-neural-networks-a-beginners-journey-into-architecture-aab30dface10.

31. Sun W, Zhao H, Jin Z. A facial expression recognition method based on ensemble of 3D convolutional neural networks. Neural Computing and Applications 2019, *31*(7): 2795-2812. https://doi.org/10.1007/s00521-017-3230-2.

32. Fang Y, Wang M, Wei L. deep transfer learning in inter-turn short circuit fault diagnosis of PMSM. 2021 IEEE International Conference on Mechatronics and Automation (ICMA) 2021; 489-494. https://doi.org/10.1109/ICMA52036.2021.9512785.

33. Yi C, Lv Y, Zhang D. A fault diagnosis scheme for rolling bearing based on particle swarm optimization in variational mode decomposition. Shock and Vibration, 2016; 2016(2): 1-10. https://doi.org/10.1155/2016/9372691.

34. Guedidi A, Guettaf A, Cardoso AJM, Laala W, Arif A. Bearing faults classification based on variational mode decomposition and artificial neural network. 2019 IEEE 12th International Symposium on Diagnostics for Electrical Machines, Power Electronics and Drives (SDEMPED) 2019. https://doi.org/10.1109/DEMPED.2019.8864830

35. De Angelo CH, Bossio GR, Giaccone SJ, Valla MI, Solsona JA, García GO. Online model-based stator-fault detection and identification in induction motors. IEEE Transactions on Industrial Electronics 2009; 56(11): 4671-4680. https://doi.org/10.1109/TIE.2009.2012468

36. Guedidi A, Laala W, Guettaf A, Zouzou SE. Diagnosis and Classification of broken bars fault using DWT and Artificial Neural Network without slip estimation. 2020 XI International Conference on Electrical Power Drive Systems (ICEPDS) 2020; 1-7. IEEE. https://doi.org/10.1109/ICEPDS47235.2020.9249315.

37. Peng D, Wang H, Liu Z, Zhang W, Zuo MJ. and Chen. J. (2020). Multibranch and Multiscale CNN for Fault Diagnosis of Wheelset Bearings Under Strong Noise and Variable Load Condition. IEEE Transactions on Industrial Informatics 2020; 16(7): 4949-4960. https://doi.org/10.1109/TII.2020.2967557.

38. Kumar P, Kumar P, Hati AS, Kim HS. Deep transfer learning framework for bearing fault detection in motors. Mathematics 2020;10:4683. https://doi.org/10.3390/math10244683

Asma GUEDIDI was born in Biskra, on January 21, 1994, she is a PhD student in the Department of Electrical Engineering at Biskra University. She received the Renewable Energy master degrees in 2016 from the University of Biskra. Her research interests include condition monitoring and fault diagnosis in electrical machines.
e-mail: guedidiasma@gmail.com

Widad LAALA was born in Biskra Algeria. She received the Electrical Engineering magisterial diploma and PHD degrees from the University of Biskra in 2005, 2016 respectively. Her research interests include condition monitoring and fault diagnosis.
e-mail: widad.laala@univ-biskra.dz

Abderrazak GUETTAF was born in Biskra, Algeria on November 28th, 1977. He received the Engineer and Magister diploma and PHD degree in electrical engineering from University of Biskra in 2002, 2005 and 2013 respectively.
e-mail: abderazakguettafok@gmail.com

Ali ARIF was born in Biskra, Algeria on June 19th, 1967. He received the Engineer, MSc diploma and PhD degree in electrical engineering from the University of Biskra, Algeria, in 1992, 2003 and 2013.
e-mail: aliarifok750@gmail.com